

## Full-length paper

***In situ* and *ex situ* electron microscopy studies of polar oxide surfaces with rock-salt structure**

Marija Gajdardziska-Josifovska<sup>1,\*</sup>, Richard Plass<sup>1,3,4</sup>, Marvin A. Schofield<sup>1,4</sup>, Daniel R. Giese<sup>1</sup> and Renu Sharma<sup>2</sup>

<sup>1</sup>Department of Physics and Laboratory for Surface Studies, University of Wisconsin Milwaukee, PO Box 413, Milwaukee, WI 53201 and <sup>2</sup>Center for Solid State Science, Arizona State University, Tempe, AZ 85287, USA, Present address: <sup>3</sup>Sandia National Laboratory, PO Box 5800, Albuquerque, NM 87185-1421 and <sup>4</sup>Brookhaven National Laboratory, PO Box 5000, Building 480, Upton, NY 11973

\*To whom correspondence should be addressed. E-mail: mgj@uwm.edu

<b>Abstract</b>	We present the fundamental problem of polar oxide surfaces and overview the different models for the stabilization of their diverging surface energy. We focus on contributions from <i>ex situ</i> and <i>in situ</i> electron microscopy and diffraction techniques toward distinguishing between competing stabilization mechanisms in oxides with rock-salt structure.
<b>Keywords</b>	polar oxide surfaces, MgO(111), NiO(111), reconstructions
<b>Received</b>	15 December 2000, accepted 8 September 2001

**Introduction**

Many issues at the frontiers of surface science and electron microscopy will be intertwined in this paper as we present an overview of the subject of polar oxide surfaces, summarize our prior publications in this area, and provide a snapshot of our recent unpublished efforts. Since the first calculation of their infinite surface energy [1], polar oxide surfaces have become the equivalent of black holes for surface science, providing a rich ground for theoretical and experimental research. Before addressing the peculiarities and particularities of polar oxide surfaces, it is worthwhile to see where they are with respect to current frontiers in our understanding of materials.

**Binaries are the frontier in surface science of oxides**

In the past few decades, surface science has invested much effort and gained a fair understanding of surfaces of elemental solids, all pointing in the direction of much richer structural behaviour compared to the bulk. The new forms of carbon are good examples of how limited dimensionality and excess of dangling bonds can lead to nano-structures that are fundamentally different from the bulk graphite and diamond. The silicon (111) surface  $7 \times 7$  reconstruction is another, now classical, example of the complexities of surface structures built even with one type of atom. The behaviour becomes even richer for surfaces and interfaces of metal alloys compound semiconductors and insulators. Whereas the bulk structures and properties of alloys and binary compounds are well understood, ternaries and above mark the frontiers in fundamental

solid state science where novel bulk properties continue to be discovered. For surfaces, however, both elemental and binary solids are the current frontiers, and we will limit our discussion here to polar surfaces of binary oxides as the simplest representative of the broad group of oxide surfaces.

Oxides and their surfaces and interfaces are of great interest in many important technologies, such as electronics, catalysis, electrochemistry, magnetic recording, superconductivity, and optics. Oxides are always present, often in uncontrolled ways, whenever a material is in contact with the ambient that prominently includes oxygen and water on our planet. Because of this, oxides are at the core of geology, they are the source ores for metallurgy, the unwanted product of corrosion, almost always present in friction and lubrication processes.

Compared to metals and unary semiconductors, the electronic properties of oxides are very diverse. Many oxides are insulators, but the family of oxides also includes wide band-gap semiconductors, ionic conductors, superconductors, ferro- and antiferroelectric and magnetic materials. The insulating oxides, with large band gaps and high melting temperatures, are often used as synonyms for ceramics. The study of their surfaces has only developed in the last decade, due to the problem of surface charging with electron and ion based characterization techniques, and due to difficulties in preparing well controlled single crystal oxide surfaces in ultra-high vacuum (UHV). Methods have been developed to circumvent some of the charging and preparation problems leading to an increased understanding, especially in the area of neutral

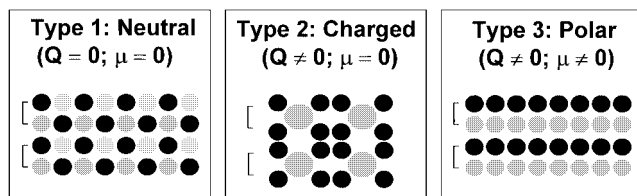


**Fig. 1** Classification of oxide surfaces into three types based on their surface charge ( $Q$ ) and dipole moment ( $\mu$ ) in the repeat unit normal to the surface (after Tasker [1]). Small light and dark circles denote cations ( $+q$ ) and anions ( $-q$ ) of equal absolute charges. Larger light circles in Type 2 denote cations with appropriately larger charge (e.g.  $+4q$  in schematic example).

oxide surfaces, as summarized in two recent books on oxide surfaces by Henrich and Cox [2] and Noguera [3]. Contrary to elemental surfaces that tend to reconstruct, the neutral surfaces of oxides tend to be close to bulk terminated structures. Furthermore, the perfect neutral surfaces are much less active compared to the oxide powders used in catalysts, both in their own right and as (active) supports for metal clusters. At present, the oxide powders are modelled as terminated by neutral surfaces with large concentration of line and point defects. A three-dimensional crystallite, however, may be terminated by a collection of low index and high index facets, which could consequently be charged or polar in addition to neutral. This increases the need to explore and understand these three classes of oxide surfaces as defined below.

### Classification of oxide surfaces

The classification scheme, due to Tasker [1], is presented in Fig. 1 for a hypothetical binary oxide. This figure is inspired by the first review paper of polar oxide surfaces by Noguera [4]. The actual ion positions and charges are defined by the crystal structure and the metal valence state. The classification is general, and can be applied to any compound material with at least partial ionic bonding. It is based on sums of charges within each of the lattice planes parallel to the surface ( $Q$ ), and the absence or presence of a dipole moment ( $\mu$ ) in the repeat unit perpendicular to the surface. Type 1 surfaces are neutral, with equal numbers of anions and cations in each plane and, hence, no dipole moment between the neutral layers. Type 2 surfaces are charged, but have no dipole moment perpendicular to the surface because of the symmetrical stacking sequence. Type 3 surfaces are polar, having a net charge within each plane and a dipole moment in the repeat unit perpendicular to the surface. This dipole moment leads to diverging sums in the electrostatic energy. As a result of this divergence, the calculated surface energy is infinite for bulk terminated polar oxide surfaces of semi-infinite ionic solids [e.g. 1,5,6] and very large even for ultra-thin films [4]. The diverging surface energy poses many interesting questions about the existence of polar oxides surfaces and the possible modes for their stabilization. By comparison, the neutral (Type 1) and charged (Type 2) surfaces have modest surface

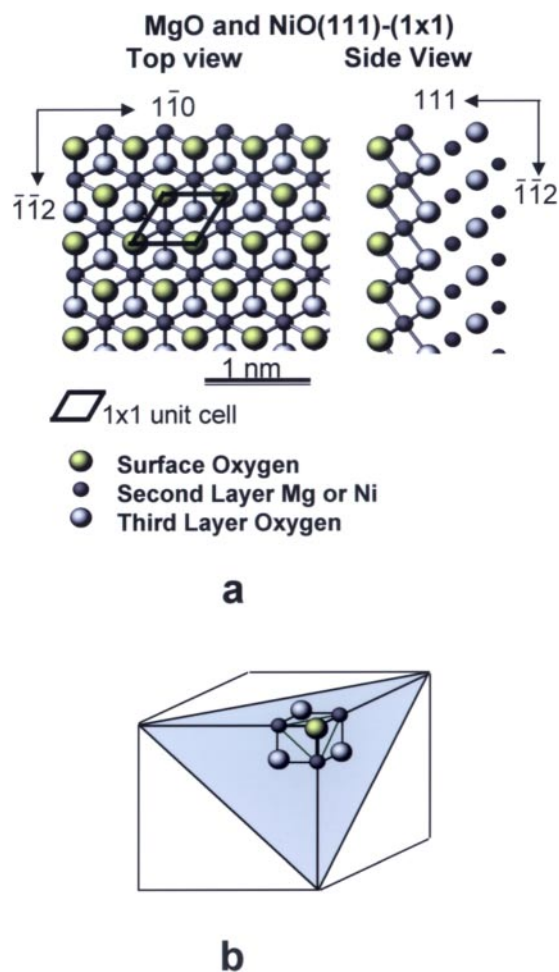


**Fig. 2** (a) Top and side view atomic model of bulk terminated (111) surface of solid with rock-salt structure. (b) Schematic representation of (111) surface, denoted in grey, and investigated models of micro-faceting and nano-faceting to neutral  $\{100\}$  planes (i.e. faces of cube). Octopolar neutral building block for rock-salt solids represents the smallest possible nano-facet, and results in  $2 \times 2$  octopolar reconstruction.

energies and can be stabilized by limited relaxation of the ions in the surface region.

### Examples of polar oxide surfaces

In the case of oxides with cubic rock-salt structure, two of the lowest index (100) and (110) type surfaces are neutral, and the (111) type surfaces are polar. The two-dimensional unit cell of the bulk-terminated (111) surface is hexagonal, with all surface ions of one kind having three dangling bonds and three-fold coordination to the underlying ions with opposite charge, as shown in Fig. 2a. In the (111) direction, planes of metal cations alternate with equidistant planes of oxygen anions. This structure is found in the alkaline-earth oxides MgO, CaO, SrO, and BaO, and in some transition-metal oxides, such as NiO, CoO, FeO, MnO, TiO, VO, and EuO. In our work, we are focusing on MgO(111) and NiO(111) surfaces as examples of polar oxide surfaces with the same bulk-terminated struc-

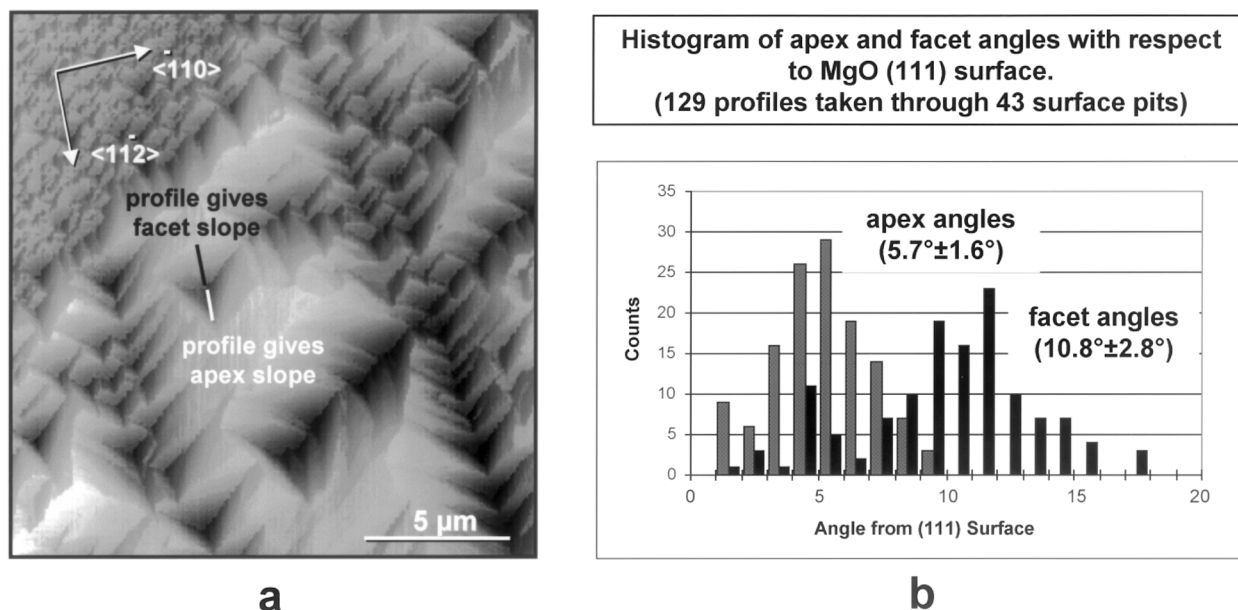


**Fig. 3** (a) AFM image of phosphoric acid etch induced vicinal faceting on single crystal MgO(111) surface. (b) Histogram of facet and apex angles measured from many AFM images. (After Plass *et al.* [10].)

tures, but differing electronic properties. MgO is the model insulating ionic oxide, while bonding in NiO is dominated by electron correlation effects. As a consequence, NiO is anti-ferromagnetic and MgO is non-magnetic. Furthermore, MgO has a much higher bulk melting temperature (2852°C) compared with NiO (1984°C), and NiO is prone to reduction both by heating in vacuum and under electron beam irradiation.

Examples of polar surfaces in other crystal systems include: (111) and (100) surfaces of inverse spinel compounds (e.g.  $\text{Fe}_3\text{O}_4$ ), the corundum (0001) surface (e.g.  $\text{Al}_2\text{O}_3$ ), wurtzite (0001) and (000-1) surfaces (e.g. ZnO), perovskite (110) and (111) surfaces (e.g.  $\text{SrTiO}_3$ ), cuprite (100) surface (e.g.  $\text{Cu}_2\text{O}$ ), and fluorite (100) surface (e.g.  $\text{ZrO}_2$ ). There are three compilations of the small number of studies of these polar surfaces [2–4] and no exhaustive lists of polar, charged, and neutral surfaces across the families of oxides. We will limit our considerations to the rock-salt oxides, and emphasize the electron microscopy methods that have been used to provide answers to some of the basic questions about polar oxide surfaces.

### Basic questions about polar oxide surfaces

The diverging surface energy of polar surfaces presents many interesting questions ranging from the fundamental ‘Can polar oxide surfaces exist?’ via the mechanistic ‘How can they be stabilized?’ to the applied ‘Would they have unique and useful surface and interface properties?’ Both theory and experiment have provided several contrary answers to the first two questions and the last is largely unexplored.

In the 1970s, the polar oxide surface problem was considered closed with consensus between theory [1] and experiment [7,8] that clean MgO(111) surfaces cannot exist but must facet into neutral {100} planes to gain finite surface

energy, as sketched in Fig. 2b. We will present the basic ideas and results behind this microfaceting model below, along with contrary results from recent microscopy studies of MgO(111) and (110) surface faceting [9–11]. Classical theory also stipulated that adsorption of charged species can lead to surface stabilization [1] and the first observation of a reconstructed NiO(111) surface was ascribed to Si impurities [12]. In the 1990s, the problem was reopened with experimental discoveries of clean reconstructed MgO(111) [13–15] and NiO(111) surfaces [16–22], and with theoretical predictions of reconstructed surfaces based on the idea of smallest neutral building blocks [5,6,23–25]. This block is an octopole for the rock-salt solids, as sketched in Fig. 2b. At present, there is disagreement between the few proposed and solved polar oxide surface structures, and the reconstruction mechanism is under construction, as presented later. The last ongoing controversy surrounds the  $1 \times 1$  structure of polar oxide surfaces. Classical electrostatic approaches predict that  $1 \times 1$  structures can exist only by adsorption of charged species [1], and some experiments have suggested hydroxyl-induced stabilization of NiO(111)  $1 \times 1$  [26–28] and MgO(111)  $1 \times 1$  [29] surfaces. In addition to confirming the general models predicted by classical electrostatic theories, quantum mechanical calculations also predict two-dimensional surface metalization of the clean  $1 \times 1$  surface [7,30,31], hitherto undetected by experiment.

### Frontiers of electron microscopy of polar oxide surfaces

The question of interest for a frontiers in electron microscopy meeting is ‘How has microscopy contributed, and how can it continue to do so, in resolving how polar oxide surfaces can shed their diverging energy and become stabilized?’ To recap,

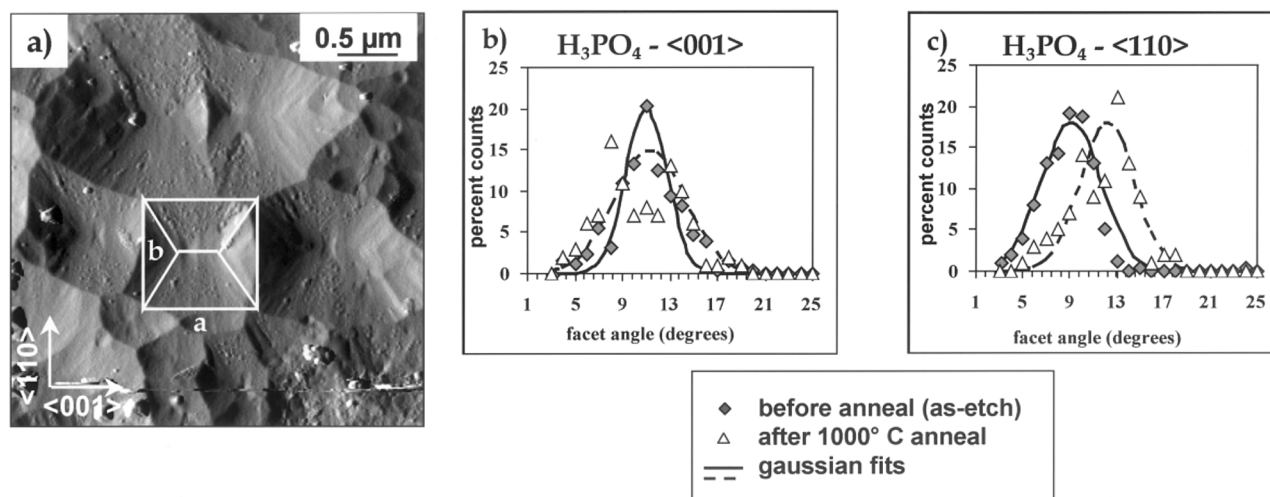


**Fig. 4** (a) AFM image from MgO(110) surface faceting induced by brief phosphoric acid etching. (b) Histograms of facet angles with respect to MgO(110), measured in two perpendicular directions after etching (solid diamonds) and after subsequent annealing (open diamonds). (After Giese *et al.* [11].)

there are four different models that are currently under consideration: (1) microfaceting into neutral planes; (2) adsorption of charged species; (3) surface reconstructions; and (4) surface metalization. As the different models span length scales from the micron to the atomic level, a combination of imaging, diffraction and spectroscopy techniques are needed, including going beyond electron microscopes to other surface sensitive techniques. In fact, very few groups have used electron microscopy techniques. These studies have included scanning electron microscopy (SEM) [8,10,11], scanning tunnelling microscopy (STM) [16,17], reflection electron microscopy (REM) in conjunction with reflection high-energy electron diffraction (RHEED) and reflection electron energy-loss spectroscopy (REELS) [13,14], surface sensitive transmission electron microscopy (TEM), and transmission high-energy electron diffraction (THEED) [15,22]. All of these applications remain at the frontiers of electron microscopy and the challenge is to combine them with *in situ* experiments under controlled atmosphere conditions and elevated temperatures. In keeping with the electron microscopy scope of these proceedings, we will emphasize these studies beyond their minority representation in the field of polar oxides. Rather than introducing all the techniques and sample preparation issues in a separate 'Experimental set-up' section, we will do so in conjunction with each of the presented results.

## Microfaceting model

### Theoretical calculations and predictions

The basic support for the faceting model comes from end point surface energy calculations. The diverging (infinite) surface energy of MgO(111) and NiO(111) surfaces can, in principle, be lowered to the smallest finite value if the polar surfaces

facet into neutral {100} faces. The neutral (100) surfaces are the lowest energy planes in the rock-salt system. For example, the calculated surface energy is 1.17 Jm<sup>-2</sup> for MgO(100) [32], and 1.74 Jm<sup>-2</sup> for NiO(100) [23]. This polar-to-neutral microfaceting requires large mass transport and, hence, high annealing temperatures in experiments. It should be noted, however, that the theoretical surface energy calculations are done at absolute zero, and cannot account for changes in surface structure and stoichiometry that occur at high temperatures, which are presented in a later section dealing with polar surface reconstructions.

### Experimental microscopy studies of surface faceting

The first SEM and low-energy electron diffraction (LEED) study of MgO(111) surfaces (prepared by acid etching, ion bombardment, and electron beam annealing (~1000°C) in UHV) reported thermal faceting into three-sided pyramids [7]. The faces of these micro-pyramids were interpreted as the neutral {100} surfaces, but without measurements of the actual facet angles due to charging effects in LEED and the inability to quantify topography from single SEM images discussed below. In conjunction with theoretical calculations of surface energies [1], these observations formed the generally accepted model that clean polar oxide surfaces undergo thermal faceting into neutral planes [2]. Following similar procedures, Onishi *et al.* [9] also reported faceting of the MgO(111) surface. Related LEED experiments with MgO(110) showed two-fold splitting interpreted as neutral-to-neutral faceting of (110) into {100} planes [7]. This faceting behaviour was in marked difference to adsorbate-induced faceting of metal semiconductor surfaces, and to reconstruction-induced stabilization of polar semiconductor surfaces. The rationalization was that oxides are more ionic than compound semiconductors and fundamentally different from metals, hence, the effects of surface

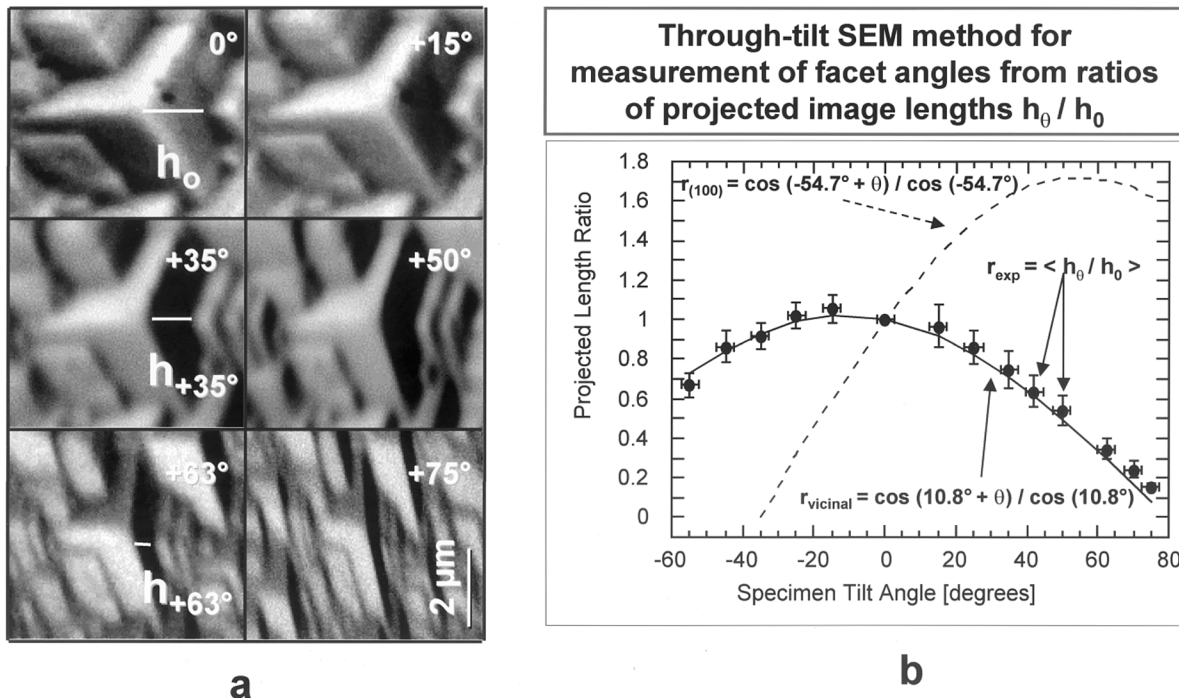


**Fig. 5** Illustration of through-tilt SEM method developed for measurement of facet angles. (a) Subset of (cropped) SEM images from same MgO(111) faceted region recorded at different specimen tilts. (b) Data points are experimental ratios ( $h_\theta / h_0$ ) of projected image lengths for same feature as function of specimen tilt angle, solid line is calculated for  $10.8^\circ$  faceting angle obtained by AFM, dashed line is calculated for  $54.7^\circ$  angle expected for {100} neutral facets. (After Plass *et al.* [10].)

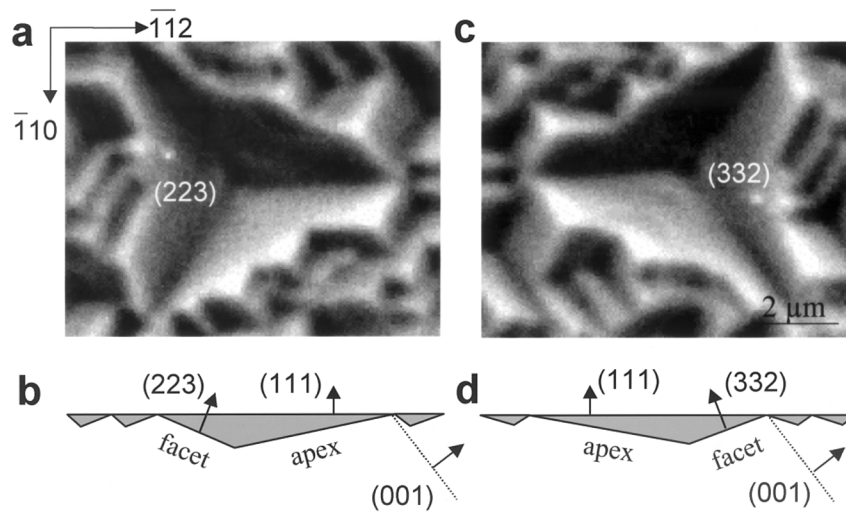


**Fig. 6** (a) and (c) Top view SEM images of nitric acid etch pits on an MgO(111) surface in the two possible orientations allowed by previous TED analysis [10]. (b) and (d) Side view schematic cross-sections of (a) and (c), illustrating the orientation of the pit walls with respect to an MgO(001) cleavage plane.

polarity in oxides might require more drastic measures to be overcome compared with polar semiconductors.

After uncovering acid-etch induced morphology on MgO(100) and (111) surfaces by REM [14], we have recently revisited the original faceting experiments of MgO(111) and (110) surfaces to find that the microfacets are induced by (hot phosphoric and nitric) acid etching and not modified by the

relatively low temperature annealing in UHV and high vacuum (HV) [10,11]. Using atomic force microscopy (AFM) and SEM to measure facet angles, we found vicinal facet planes rather than the expected {100} planes. For example, Fig. 3a illustrates the case of triangular pyramids on an MgO(111) surface that was mechanically polished to  $0.25 \mu\text{m}$  diamond, etched for 30 s in  $185^\circ\text{C}$  phosphoric acid, briefly  $\text{Ar}^+$  sputtered,

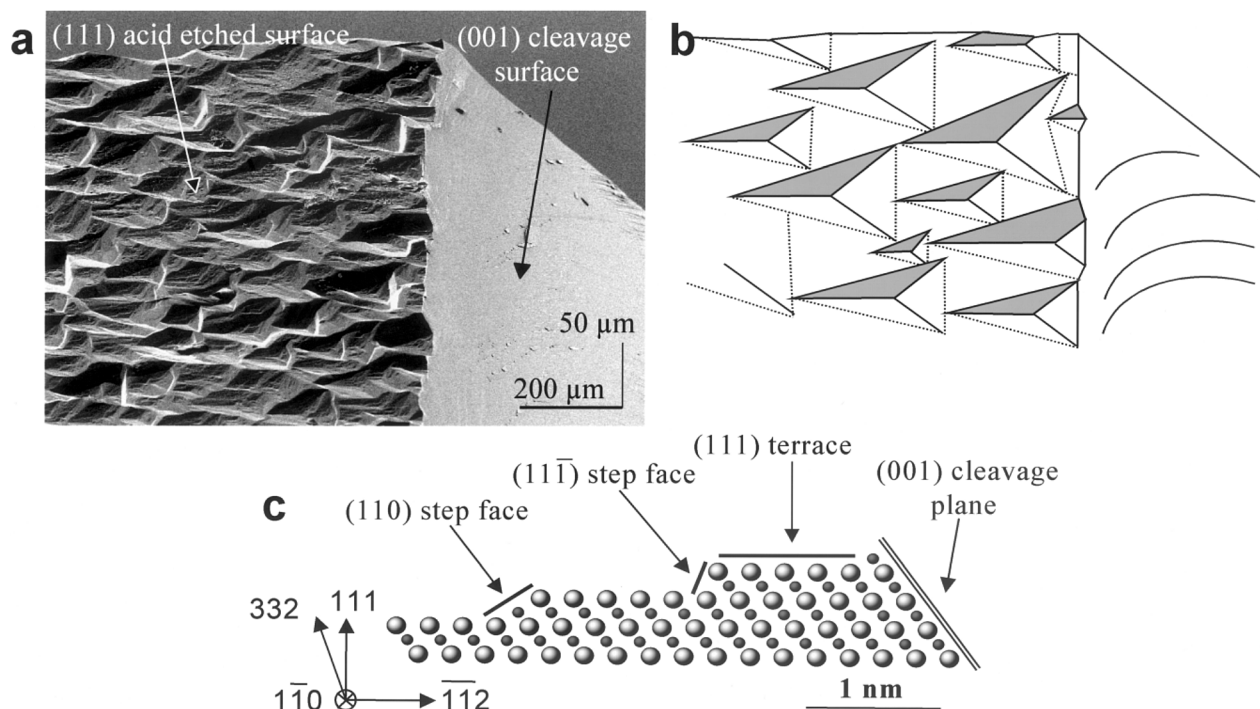


**Fig. 7** (a) Perspective view scanning electron micrograph of a nitric acid etched MgO(111) surface that has been subsequently cleaved and Au/Pd coated to reduce sample charging. The etch induced depressions are pointing away from the 100 cleavage plane indicating that they are at angles statistically distributed about {332} vicinal planes, as illustrated in (b) a comparable perspective view schematic of the sample, and in (c) possible side view atomic level model of an oxygen terminated MgO(332) surface with two surface step face configurations.

and then e-beam annealed (from back side) at 1050°C for 5 min in UHV. The average facet angles were measured by AFM to be  $10.8 \pm 2.8^\circ$  from the (111) plane both before annealing (not shown here) and after annealing (Fig. 3b), in marked difference from the  $54.7^\circ$  angle between {100} planes and the (111) surface [10]. The measured apex angles of  $5.7 \pm 1.6^\circ$  further confirm that these triangular pyramids are shallow. A richer time-dependent acid-etch behaviour was observed on the MgO(110) surfaces, where quantitative AFM (and SEM) measurements find a wider range of facet angles ( $9\text{--}23^\circ$ ), again shallower than the expected  $45^\circ$  and  $90^\circ$  {100} facet angles [11]. The example in Fig. 4a is from MgO(110) surface after short etching times in hot phosphoric acid. The facet angle histograms in Figs 4b and 4c show similar average angles before and after annealing at 1000°C, confirming again that this faceting cannot be treated in the usual context of thermal equilibrium at a solid/vacuum interface. Instead, the faceting is driven by reactive solid/liquid interface kinetics.

#### Through-tilt SEM method for measurement of facet angles

Questions about AFM tip convolution effects are important in quantitative measurements of facet angles, and we have developed a SEM method to measure facet angles on these oxide surfaces. While the shallow escape depth of secondary electrons provides a stunning impression of 3D surface topography in SEM images, one cannot measure faceting angles

from a single SEM image taken in arbitrary orientation. However, by tilting around an axis that coincides with a facet edge direction, and recording a series of images at different tilts, we have been able to extract the facet angle information for both MgO(111) and MgO(110) surfaces [10,11]. The method was first described by Plass *et al.* [10], and its essence is illustrated in Fig. 5 for MgO(111). In this case, the sample holder's tilt axis was aligned parallel to one of the crystal's  $\langle 110 \rangle$  directions, which was determined from TEM and diffraction studies of equivalently faceted samples. In the Topcon ABT-32 SEM instrument used, the electron beam impinges perpendicularly on a sample laid flat; we take this to be a tilt angle of  $0^\circ$ . A positive tilt angle is taken to indicate the facet of a pyramidal pit turned towards the incident beam. A subset of (cropped) images in Fig. 5a, illustrates the reduced projected dimension ( $h_\theta$ ) of a facet as function of tilt angle ( $\theta$ ). Normalizing by the projected facet size at zero tilt ( $h_0$ ), we calculate size-independent ratios  $h_\theta / h_0$ , which are averaged over a large number of measured facets. The facet angle ( $\alpha$ ) can then be obtained from the equation:

$$\frac{h_\theta}{h_0} = \frac{\cos(\alpha + \theta)}{\cos \alpha}$$

The solid line in Fig. 5b is calculated from the above equation based on the average faceting angle ( $\alpha = 10.8^\circ$ ) measured by AFM, while the dashed line is calculated for the {100} faceting model ( $\alpha = 54.7^\circ$ ). The data points and associated errors

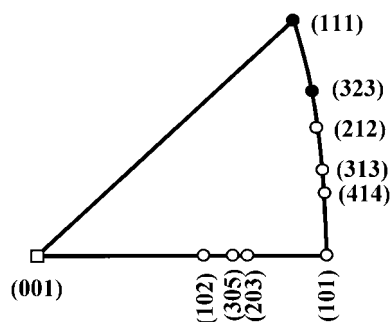


**Fig. 8** Stereographic triangle with summary of experimentally measured acid-etch induced faceting planes on MgO(111) surface (after Plass *et al.* [10] and information in this paper; starting and ending planes are denoted by closed circle), and MgO(110) surface (after Giese *et al.* [11]; starting and ending planes are denoted by open circle). These are drastically different from the expected {100} planes for thermal faceting (denoted by open square).

are experimental averages of  $h_0/h_0$  from several pits imaged by through-tilt SEM. In this case, the SEM clearly confirms the AFM results and disproves the {100} faceting model. While AFM provides easier measurements of vicinal facet angles on insulating surfaces, the through-tilt SEM method would be invaluable for quantification of steeper facet angles when tip convolution could be limiting for AFM. Tilting errors and the needed conductive coating of insulating samples are the main limitations of this SEM method.

### How to resolve a 180° ambiguity in SEM?

Knowledge of the facet edge directions from TEM and THEED, and facet angles from AFM and SEM, leaves a 180° ambiguity in determination of the actual facet planes for the MgO(111) surface. This ambiguity is illustrated in Fig. 6, indicating that the pyramid faces could be formed from either mainly {223} facet planes (shown in Figs 6a and 6b at 11.4° from the (111) surface towards the (001) surface), or mainly {332} facet planes (shown in Figs 6c and 6d at 10.0° from the (111) surface *but in the opposite direction* from the (001) surface). Here we show a novel SEM experiment which removes this ambiguity by imaging MgO(111) crystals that have been acid etched and subsequently cleaved to provide a needed crystallographic direction standard.

Figure 7a shows a representative low magnification SEM image of a nitric acid etched (111) surface (left side) and the cleaved (001) surface (right side), along with its schematic representation in Fig. 7b. The left sides of Figs 7a and 7b show that the shallow, triangular etch pits on the (111) surface point away from the (001) cleavage plane of MgO. This fact reveals that the vicinal facet planes are (on average) {332} planes, inclined towards the *higher* surface energy {110} planes, as opposed to {223} planes inclined towards the lower surface energy {001} planes, again demonstrating that acid-induced faceting is fundamentally different from thermal equilibrium faceting. The results from the (111) and (110) studies are

summarized in stereographic representation in Fig. 8.

In the current *ex situ* AFM and SEM experiments, the atomic structure of the final vicinal facets remains unresolved. Are they indeed similar to the idealized (332) model in Fig. 7c? Do they have double steps, presenting the same ion to the surface, or single steps that could give a new stabilization mechanism of alternating terraces of positive and negative charge? Do their step faces have a {110} or {111} character? Do they have {100} short range facet character at length scales that are beyond the current resolution of SEM and AFM? *In situ* microscopy studies with atomic resolution are needed to make further progress in the understanding of these high index faceted surfaces. Such acid-etch-generated surfaces could provide new model systems for understanding growth and catalytic reactions on stepped oxide surfaces with mixed polar and neutral character. One can imagine a number of interesting polar semiconductor or organic structures grown on such polar oxide substrates with nanometre scale constraints provided by their limited terraces.

### Summary of faceting results

Microscopy has played a crucial role in the experimental investigation of the polar-to-neutral faceting model for the stabilization of polar oxide surfaces. The first SEM images, showing three-sided pyramids on MgO(111) surfaces [7], were taken to be proof of the microfaceting model based on symmetry. The accepted model was that clean polar oxide surfaces undergo thermal faceting (in UHV) to neutral planes, as reviewed in books on oxide surfaces [2,3]. Our recent AFM and SEM measurements of faceting angles have disproved the model [10,11]. The measured faceting angles are consistent with higher index (vicinal) planes, as summarized in Fig. 8. This vicinal polar surface faceting is induced by acid etching, it is not promoted by annealing at the relatively low temperatures used by prior researchers and it is erased at high temperatures by a competing process of polar oxide surface reconstruction [10,15].

## Reconstruction stabilization of polar oxide surfaces

### Reconstructed surface types and their accessibility for electron microscopy

Apart from contributing towards the construction and deconstruction of the microfaceting model, electron microscopy and diffraction have contributed to the current understanding of non-faceted polar oxide surfaces. In an above section, we introduced the proposed stabilization mechanisms for such flat surfaces via surface reconstruction, adsorption of charged species, and surface metalization. All of these mechanisms involve some combination of changes in the surface stoichiometry and bonding, with consequences to the surface atomic structure. We will use the term 'reconstructed surface' to indicate a clean or adsorbate-stabilized surface with in-plane ( $x$ - $y$ ) periodicity  $m \times m$  different from a bulk terminated  $1 \times 1$

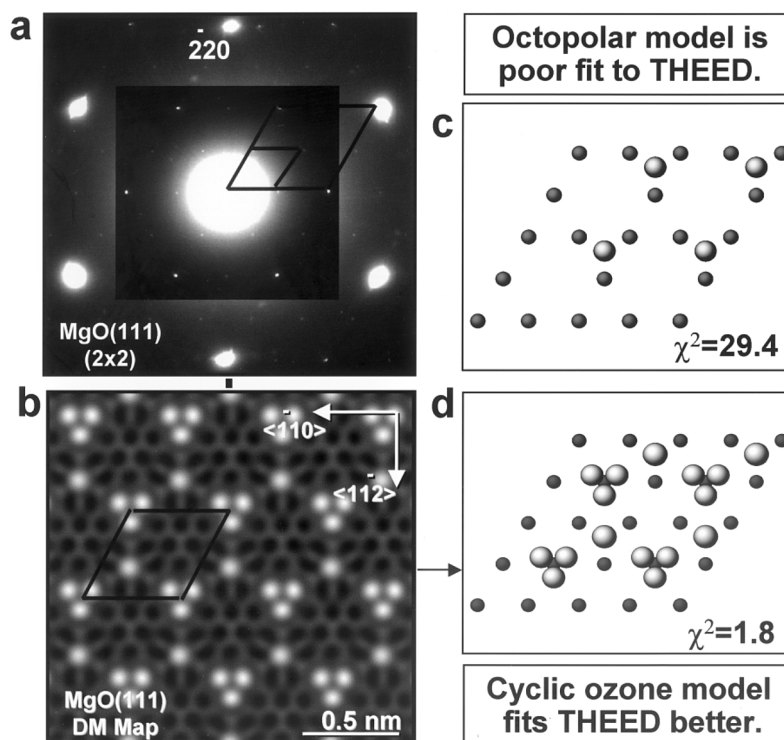


**Fig. 9** (a) Experimental THEED pattern from MgO(111)-(2x2) surface reconstruction obtained by vacuum annealing. Larger rhombus indicates cell of unreconstructed 1x1 surface, while smaller rhombus indicates the actual 2x2 surface periodicity. (b) Direct methods map with pronounced trimer and single peaks results in cyclic ozone atomic model (d), which is better fit than octopolar model (c). (After Plass *et al.* [15].)

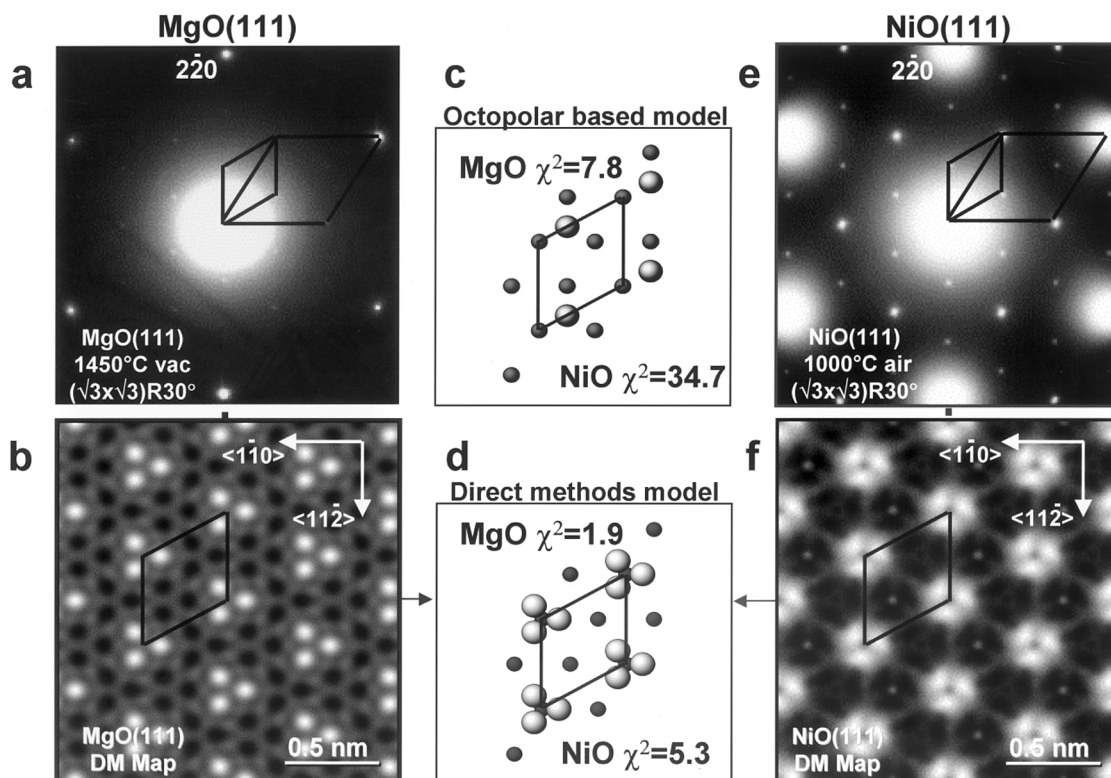


**Fig. 10** (a) and (e) Experimental THEED patterns from MgO(111)- and NiO(111)-( $\sqrt{3} \times \sqrt{3}$ )R30° reconstructions, with denoted bulk terminated and reconstructed cells. (b) and (f) Direct method maps with pronounced trimers resulting in cyclic ozone atomic models (d) that are better fits to the experimental data than octopolar inspired ( $\sqrt{3} \times \sqrt{3}$ )R30° model. (MgO data are after Plass *et al.* [15] and NiO data are unpublished.)

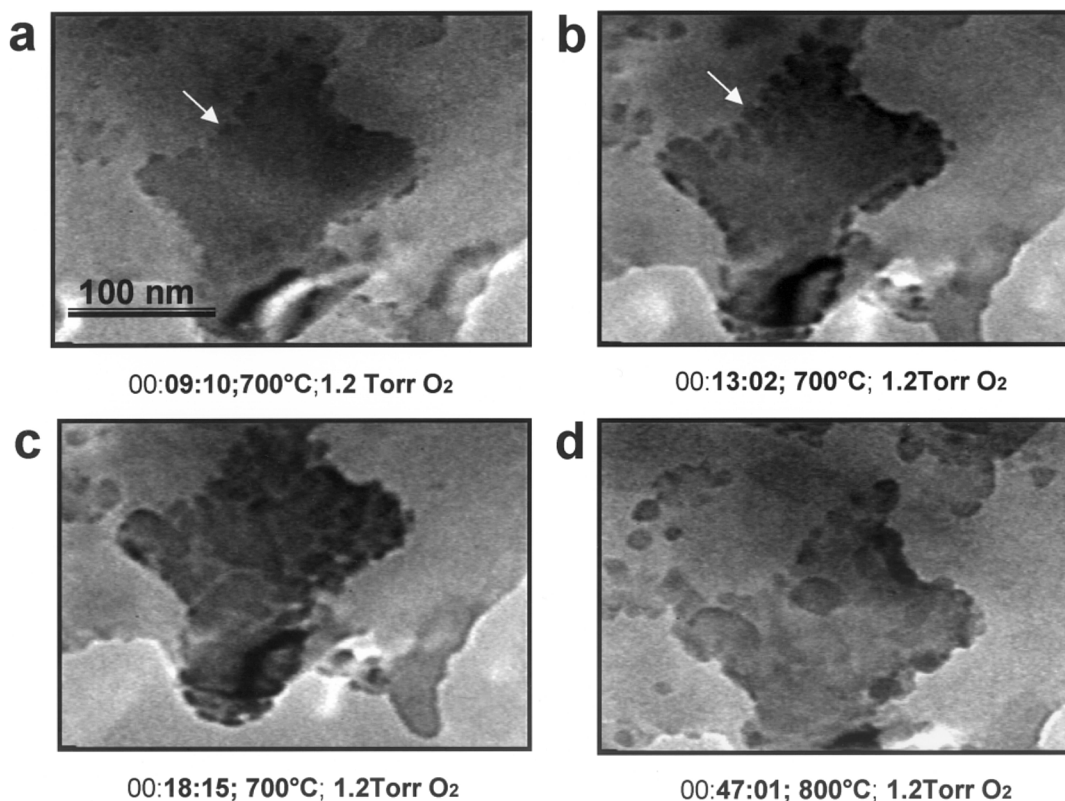


**Fig. 11** *In situ* ETEM imaging of  $(\sqrt{3} \times \sqrt{3})R30^\circ$  reconstruction development on NiO(111) surface at 1.2 Torr oxygen pressure and at 700–800°C temperatures. Images are excerpts from video recording showing that reconstruction nucleates and grows from terrace edges (arrowed in initial two images).

structure. Such surfaces show extra reflections in their RHEED and THEED patterns, and the first part of this section will be devoted to electron diffraction from clean reconstructed surfaces. REM and profile- and plan-view TEM provide additional information on the terrace and step morphology, while REELS and EELS can give compositional and bonding information. The problem in all cases is that the small surface signal is superimposed on the large bulk signal, necessitating special surface optimized variants of these microscopy techniques. The existing surface-specific THEED techniques reach their limit for  $1 \times 1$  surface structures that can have only changes in the interlayer (*z*) spacing. We currently use photoelectron diffraction to study the  $1 \times 1$  structures, but these studies are beyond the scope of this paper. For completeness we will include references for the  $1 \times 1$  polar oxide surface structures without showing results, and focus on the reconstructions with larger surface periodicity.

Additional experimental considerations arise from the special environmental requirements for oxide surface studies, which are substantially different from the UHV requirements for studies of unary surfaces. The standard UHV methodology was primarily developed to prevent the oxidation of unary metal and semiconductor surfaces, and most of the *in situ* surface-cleaning techniques were designed to remove the oxides from surfaces exposed to Earth's atmosphere. Hence, the UHV

paradigm is exactly opposite from the needed oxygen-rich environment for formation and/or maintenance of oxide surfaces. Development of environmental TEM (ETEM) instruments, in which oxide surfaces can be observed and heated under a few Torr of oxygen, provide a new environment for oxide surface studies. In this paper we will present preliminary data from the first *in situ* ETEM study of oxide surface reconstructions.

### Early history of polar oxide surface reconstructions

The first TEM, SEM, and STEM observations of NiO crystallites with octahedral shapes by Pease *et al.* [33] and Cowley [34] showed that the {111} polar faces can be stabilized at least in small crystallites. It was noted that in presence of Si these NiO octahedra grow in size to the micron range [33], but their surface structure and purity remained unknown. These microscopy observations inspired the first RHEED study of bulk NiO(111) surfaces by Floquet and Dufour [8], who discovered the first reconstruction stabilized NiO(111)- $(\sqrt{3} \times \sqrt{3})R30^\circ$  surface. Auger electron spectroscopy showed the presence of Si, and the reconstruction was attributed to a formation of a surface spinel. Prior to these experiments, the only observation of a polar rock-salt surface was on thin films of CoO(111) obtained by oxidation of Co(0001) [35,36], with LEED data indicative of O terminated and contracted clean

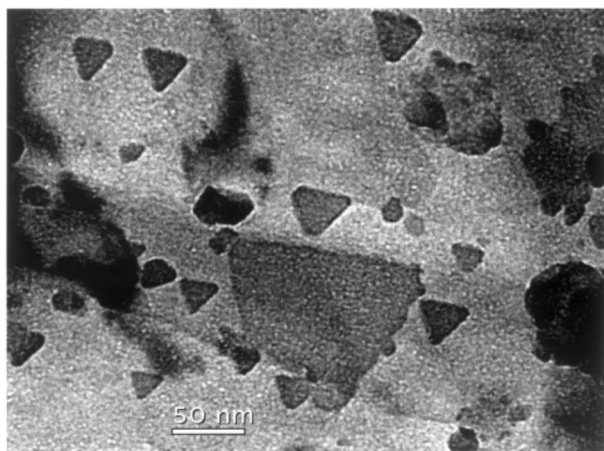


**Fig. 12** Triangular surface domains on NiO(111)-( $\sqrt{3} \times \sqrt{3}$ )R30° surface after 800°C annealing in 1.2 Torr oxygen in an environmental TEM.

surface. The first author of this paper was involved in the next surprising experimental discovery of air-stable MgO(111)-( $\sqrt{3} \times \sqrt{3}$ )R30° surfaces by RHEED, REM, and REELS [13,14]. This reconstruction was formed by prolonged high temperature (1500–1700°C) anneals under atmospheric pressure of pure oxygen. REELS studies showed that the reconstructed MgO(111) surface is oxygen rich in comparison to the neutral MgO(100) surface [13]. The reconstructed MgO(111) surface did not show detectable Ca, except in isolated three-dimensional islands, contrary to pronounced one-dimensional Ca segregation to the steps of the neutral MgO(100) surfaces annealed under identical conditions [37,38].

While the early experimental results on flat CoO, NiO, and MgO(111) surfaces were different, they stimulated reconsideration of the problem of polar oxide surfaces that, until the early 1990s, was considered closed by the neutral faceting model. The ensuing theoretical revisit of the Madelung energy problem by Wolf [5] provided the impetus by predicting a 0 K octopolar ( $2 \times 2$ ) reconstruction on (111) surfaces of rock-salt solids. The growing number of recent references on reconstructed polar oxide surfaces indicates a revival of this field. While the first two books on oxide surfaces, published in 1994 [2] and 1996 [3], were dominated by the microfaceting model for polar oxides, the first review paper on polar oxide surfaces, published in 2000 [4], is dominated by reconstructions.

### Octopolar theoretical model

The reconstruction mechanism allows changes in the surface stoichiometry and/or bonding by changing the surface periodicity from bulk-terminated. For example, the theoretical octopolar ( $2 \times 2$ ) structure is obtained by removing three-quarters of the top layer ions and one-quarter of the second layer ions [5], as shown schematically in Fig. 9c. This is equivalent to building the rock-salt solid with its smallest neutral building block, which is one-eighth of its bulk unit cell containing four ions of each kind. The dipole and quadrupole

moments vanish, leaving an octopole moment, and hence the name of the reconstruction. We show the octopolar unit in Fig. 2b, overlaid on the micro-faceting scheme, to emphasize that it is made of the smallest possible {100} nano-facets. In the case of a semi-infinite NiO crystal, the calculated infinite surface energy for a bulk terminated NiO(111)-( $1 \times 1$ ) surface is reduced to  $4.3 \text{ Jm}^{-2}$  for the octopolar NiO(111)-( $2 \times 2$ ) surface [23]. Models that incorporate the octopolar ‘nano-faceting’ idea have been calculated also for MgO(111) with ( $2 \times 1$ ) [6], ( $\sqrt{3} \times \sqrt{3}$ )R30° [25], ( $2 \times 2$ ) [6], and ( $2\sqrt{3} \times 2\sqrt{3}$ )R30° [25] periodicity. In addition to the RHEED observations of MgO(111)-( $\sqrt{3} \times \sqrt{3}$ )R30° [13,14], the last three reconstructions were observed recently by our group in THEED patterns from thinned and vacuum annealed MgO (111) single crystals [15]. In the next section we will summarize our MgO(111) reconstruction results and present the equivalent unpublished results for NiO(111) obtained by electron microscopy and diffraction.

### Experimental structure determinations for reconstructed MgO and NiO (111) surfaces using direct methods for transmission high-energy electron diffraction

RHEED enabled the discoveries of reconstructed MgO(111) and NiO(111) surfaces, but the data include multiple scattering effects that must be analysed by dynamical theory. In the first structure determination for the MgO(111) reconstructions [15] we chose THEED, a surface variant of selected area diffraction (SAD), to allow use of the simpler kinematical theory. The single scattering approximation is valid for THEED data from reconstructed surfaces when they are tilted away from a bulk zone axis. This approach follows the pioneering work of Takayangi *et al.* [39] that solved the famous Si(111)-( $7 \times 7$ ) structure from THEED data. The second reason for choosing THEED was to take advantage of the recent developments of direct methods for electron surface crystallography in the group of Marks [40 and references therein]. Detailed description of the principles and many numerical algorithms used in direct methods is beyond the scope of this paper. We will only illustrate how direct methods are applied to the problem of polar oxide surfaces.

Figure 9 illustrates the structure determination approach, which starts with an experimental THEED pattern (Fig. 9a) recorded from a reconstructed MgO(111)-( $2 \times 2$ ) surface that is tilted away from the [111] zone and any of the 220 and 422 type Kikuchi lines. The samples are 3 mm discs cut from single crystals of MgO, polished, dimpled, and Ar<sup>+</sup> ion milled, then annealed in an MgO lined tungsten boat vacuum furnace ( $\sim 10^{-7}$  Torr) to successively higher temperatures above 1450°C, resulting in stabilization of the ( $\sqrt{3} \times \sqrt{3}$ )R30°, ( $2 \times 2$ ), and ( $2\sqrt{3} \times 2\sqrt{3}$ )R30° reconstructions with increasing temperature [15]. The air-stability of these structures allows transport through air and observation in our standard high vacuum Hitachi H-9000NAR microscope. When recording on film (used for both MgO and NiO THEED data), we use a

through-exposure series to capture the high dynamic range of the pattern and to correct for film non-linearity. The exposure series is then used to quantify the *reconstruction specific* beam intensities with a cross correlation technique [41]. To take advantage of the high linear dynamic range offered by CCD detectors, we have developed a tableau method for recording digital THEED data at large cameral lengths on a  $1024 \times 1024$  slow scan CCD camera. This method allows measurements to higher scattering angles while maintaining sufficient sampling of each reconstruction spot [22]. The CCD method was used for NiO(111) THEED intensities and compared favourably to the data recorded on film from the same surface [22].

After quantification of the experimental diffraction intensities, standard structure analysis builds models of candidate structures, calculates the diffraction amplitudes of each model by kinematical or dynamical theory, and compares these calculated patterns against the experimental pattern. An  $R$  or  $\chi^2$  factor is used to estimate which of the models presents the best fit and the best candidate models are further refined, by varying the atomic coordinates, to minimize the value of the factor. The application of this approach to the  $2 \times 2$  THEED data in Fig. 9a yields a high  $\chi^2$  value for the proposed octopolar structure depicted in Fig. 9c, indicating poor fit to experiment. The fundamental limitation in this structure solution approach stems from the loss of phase information when diffraction data is recorded. A secondary limit stems from an uncertainty that all possible viable models have been imagined and tested. This limit is accentuated in the new field of polar oxide surfaces, which does not have a knowledge base of solved surface structures to be used as guides. Direct methods, on the other hand, provide numerical procedures for retrieval of the lost phases, yielding possible phase data sets that are consistent with the symmetry of the pattern. The new complex diffraction amplitudes can be Fourier transformed to obtain real-space maps of the scattering potential, and hence the projected atom locations. These maps provide additional model structures, which may not have been previously imagined, that can be refined by the  $\chi^2$  kinematical procedure outlined in the beginning of this paragraph. In the case of the MgO(111)- $(2 \times 2)$  structure, the best direct methods map is shown in Fig. 9b and the resulting model, with a greatly reduced  $\chi^2$  value, is shown in Fig. 9d. The top layer  $2 \times 2$  surface unit cell of our model consists of a single oxygen ion bonded to three equidistant Mg ions in the second layer, and a single oxygen trimer placed directly above the underlying Mg ion [15]. The distance between the trimer oxygens is in the range consistent with bond lengths of ozone, where the triangular closed form is known as *cyclic ozone*. Whereas cyclic ozone is not stable in its free form (see discussion and references in [15]), bonding to the MgO(111) surface appears to stabilize both the polar surface and the cyclic ozone.

The same experimental approach was used to obtain and analyse the other two MgO(111) reconstructions obtained by annealing in vacuum [15]. In Fig. 10a we show one such THEED pattern from the MgO- $(\sqrt{3} \times \sqrt{3})R30^\circ$  reconstruction,

its direct methods map in Fig. 10b and the best fit (cyclic ozone) model in Fig. 10d. Again, the fit to the octopolar inspired model (Fig. 10c) is poorer. We have been able to produce the MgO(111)- $(\sqrt{3} \times \sqrt{3})R30^\circ$  reconstruction by high temperature annealing of both large and thinned single crystals, by use of different heating methods, under oxygen pressures ranging from atmospheric to UHV, and under both *ex situ* and *in situ* observation conditions. This is in marked difference to NiO(111), which reduces when annealed in vacuum. The NiO(111)- $(\sqrt{3} \times \sqrt{3})R30^\circ$  reconstruction shown in Fig. 10e was produced by annealing at  $1000^\circ\text{C}$  in air. The onset of the reconstruction at  $\sim 650^\circ\text{C}$  is at a much lower temperature compared to the  $\sim 1450^\circ\text{C}$  needed for formation of the same reconstruction on MgO(111). Regardless of the electronic structure differences between NiO and MgO, reflected in the temperature and oxygen pressure differences needed to form their  $(111)$ - $(\sqrt{3} \times \sqrt{3})R30^\circ$  reconstructions, the NiO direct methods map (Fig. 10f) and best structure solution (Fig. 10d) is consistent with the MgO(111)- $(\sqrt{3} \times \sqrt{3})R30^\circ$  cyclic ozone model [22,42].

The theoretical octopolar models considered in each of the structural analyses above are constructed in a purely ionic picture that allows only bonding between opposite ions (i.e. Mg to O). In our experimentally derived structures, however, the oxygen-to-oxygen distance in the top plane is small enough to allow formation of a cyclic ozone molecule, which is then bound to the underlying Mg ions. Hence, in addition to the Mg-O bonds, we should have Mg-O<sub>3</sub> bonds. At present, the nature and charge of the magnesium-ozone bond is unknown. If we adopt a purely ionic picture, and use the simplest charge balance criterion that the charge density of the top layer needs to be half of the opposite charge density for the underlying layer [4], we cannot obtain the same cyclic ozone ionicity in all MgO reconstruction models. For example, the  $(\sqrt{3} \times \sqrt{3})R30^\circ$  structure of Fig. 10d has one O<sub>3</sub> molecule per unit cell in the first layer, over three Mg<sup>+2</sup> ions per cell in the second layer. To balance the net  $+6|e|$  charge of these Mg ions, the cyclic ozone needs to have a charge O<sub>3</sub><sup>-3</sup>. Similarly, for the  $(2 \times 2)$  cell in Fig. 9d, if we keep the single oxygen ion with its usual charge of O<sup>-2</sup>, we need to assume a charge of O<sub>3</sub><sup>-2</sup> (for a total charge per surface unit cell of  $-4|e|$ ) to balance the underlying four Mg<sup>+2</sup> ions. Finally, for the  $(2\sqrt{3} \times 2\sqrt{3})R30^\circ$  cell consisting of one oxygen trimer at the corner, three oxygen ions at regular lattice sites and three oxygen ions at stacking fault sites [15], we need neutral O<sub>3</sub> to balance the 12 Mg<sup>+2</sup> ions, implying a purely covalent bond. This variation from O<sub>3</sub><sup>-3</sup> to O<sub>3</sub><sup>-2</sup> to O<sub>3</sub><sup>0</sup> is highly unphysical, taking into consideration the similar location of O<sub>3</sub> in all three reconstructions.

Hydrogen is not considered in the current structural models for reconstructed MgO and NiO because its contributions to the diffracted intensities are comparable to the noise. Nevertheless, our recent high-resolution XPS studies of MgO(111)- $(1 \times 1)$  structures show oxygen 1s shifts that are indicative of O-H surface bonds [29]. These studies are performed *in situ*, after oxygen plasma cleaning and  $800^\circ\text{C}$  annealing in  $\sim 10^{-11}$

Torr, in a Pacific Northwest National Laboratory's UHV system optimized for oxide surface science. Whereas neutral MgO(100) surfaces are prepared in the same system without traces of hydrogen, the polar MgO(111)- $1 \times 1$  surface, not having the freedom to change its surface periodicity at the low annealing temperatures used, appears to be an efficient absorber of hydrogen. Allowing, therefore, for hydrogen in the reconstructed surfaces, we can achieve consistent charge balance in all three model structures if we assume that the surface hydrogen bonds only to the single oxygen ions located at the regular bulk terminated (i.e.  $1 \times 1$ ) sites, but not to the stacking fault or cyclic ozone oxygens. The cyclic ozone would then have a charge of  $-3$  in all three reconstructions. The detection of hydrogen in surface structures is at the boundary of current surface diffraction techniques, and the role of hydrogen in the stabilization of polar oxide surfaces is an open, hot issue.

### *In situ* environmental TEM formation and observation of NiO(111) surface reconstruction

In this final section, we present a brief glimpse in the new facility provided by environmental cell TEM to produce and observe the NiO(111) reconstruction *in situ*. Several TEM instruments around the world have been modified to include differentially pumped environmental cells at the specimen stage, admitting higher gas pressures around the specimen while the rest of the microscope is kept at a safe operational vacuum that allows *in situ* dynamical studies [e.g. 43,44 and references therein]. Sharma and collaborators at Arizona State University have developed two such ETEM instruments [45,46], and applied them to a range of materials problems. Here, we show that ETEM can be applied to produce and observe surface reconstructions on oxide surfaces that reduce when heated in vacuum, as is the case with the NiO(111) polar surface.

The NiO(111) TEM sample was prepared by mechanical dimpling followed by ion milling and annealing in air to form the  $(\sqrt{3} \times \sqrt{3})R30^\circ$  structure. Before travelling to Arizona State University, the sample was kept in air at the University of Wisconsin, Milwaukee, and then at Brookhaven National Laboratory for several months. Prior to insertion in the Philips 430 ETEM, the sample and heating holder were plasma cleaned for 10 min in an EAF plasma cleaner using  $\sim 50$  mTorr oxygen (25%) and argon (75%) mixture. After all these treatments, it is notable that the strongest low angle spots of the  $(\sqrt{3} \times \sqrt{3})R30^\circ$  structure were still detectable in the THEED patterns recorded on film [47]. This extreme stability of the reconstruction to air and gas plasma was matched by our prior observation that the reconstruction survives even after dipping of the annealed NiO(111) TEM sample in cold nitric acid [22], and is consistent with one of the important applications of NiO as a corrosion-resistive coating. The remnants of the reconstruction were gradually removed in the ETEM experiments by *in situ* annealing in 1.2 Torr oxygen, and only  $1 \times 1$  spots with faint rings were recorded at  $600^\circ\text{C}$ . Increasing the temperature

above  $665^\circ\text{C}$  initiated formation of the  $(\sqrt{3} \times \sqrt{3})R30^\circ$  structure, determined by *in situ* observation of THEED patterns, both at high temperature and after the sample was quenched from  $800^\circ\text{C}$  to room temperature. Bright-field TEM images, with the sample tilted away from zone and systematic row orientations to maximize surface contrast, were recorded on video while the sample was held at elevated temperatures in the presence of oxygen. Figure 11 illustrates four such images that show the nucleation of the reconstructed surface domains at terrace edges, with their subsequent growth to coalescence. Nucleation also occurs on the extended terraces, resulting in higher density of new triangular features upon prolonged *in situ* annealing in oxygen, as shown in Fig. 12. These preliminary results demonstrate that ETEM, in combination with electron diffraction and spectroscopy, provides a new environment for study of oxide surface reconstructions.

### Discussion of reconstruction mechanism for MgO(111) and NiO(111) polar oxide surfaces

The atomic models reviewed above are the first and only structure solutions for MgO(111)- $(\sqrt{3} \times \sqrt{3})R30^\circ$ ,  $(2 \times 2)$ , and  $(2\sqrt{3} \times 2\sqrt{3})R30^\circ$  surfaces, and for the NiO(111)- $(\sqrt{3} \times \sqrt{3})R30^\circ$  to date. These structures do not fit the octopolar  $2 \times 2$  theoretical model of Wolf [5] and its related nano-faceting variants, yet the first GIXD structure solution for NiO(111)- $(2 \times 2)$  supports the octopolar theoretical model [21]. This seeming contradiction is not unusual for surface science, in which structures are established only after investigated by many different techniques and reproduced in many different laboratories. In the new field of polar oxide surface reconstructions this process has just begun, and questions outnumber the currently available answers.

### Concluding remarks

Polar oxide surfaces pose an interesting singularity, which has attracted much recent attention after it was demonstrated that these surfaces do not have to facet to neutral planes to remove their diverging surface energy. The current emerging picture is that polar oxide surfaces are stabilized by surface reconstructions at higher temperatures, and by hydroxyl  $1 \times 1$  structures at lower temperatures. The current frontier is in determining the structural models for these reconstructions, their properties, and their potential applications.

### References

- 1 Tasker P W (1979) The stability of ionic crystal surfaces. *J. Phys. C: Solid State Phys.* **12**: 4977–4984.
- 2 Henrich V E and Cox P A (1994) *The Surface Science of Metal Oxides*. (Cambridge University Press, Cambridge.)
- 3 Noguera C (1996) *Physics and Chemistry at Oxide Surfaces*. (Cambridge University Press, Cambridge.)
- 4 Noguera C (2000) Polar oxide surfaces. *J. Phys.: Condens. Matter* **12**: R367–R410.
- 5 Wolf D (1992) Reconstruction of NaCl surfaces from a dipolar solution to the Madelung problem. *Phys. Rev. Lett.* **68**: 3315–3318.

- 6 Pojani A, Finocchi F, Goniakowski J, and Noguera C (1997) A theoretical study of the stability and electronic structure of the polar {111} face of MgO. *Surf. Sci.* **387**: 354–370.
- 7 Henrich V E (1976) Thermal faceting of (110) and (111) surfaces of MgO. *Surf. Sci.* **57**: 385–392.
- 8 Floquet N and Dufour L-C (1983) Stability and reactivity of (001) and (111) NiO: RHEED-AES investigation of surface segregation and Ni formation by gas reduction. *Surf. Sci.* **126**: 543–549.
- 9 Onishi H, Egawa C, Aruga T, and Iwasawa Y (1987) Adsorption of Na atoms and oxygen-containing molecules on MgO (100) and (111) surfaces. *Surf. Sci.* **191**: 479–491.
- 10 Plass R, Feller J, and Gajdardziska-Josifovska M (1998) Morphology of MgO (111) surfaces: artifacts associated with the faceting of polar oxide surfaces into neutral surfaces. *Surf. Sci.* **414**: 26–37.
- 11 Giese D R, Lamelas F J, Owen H A, Plass R, and Gajdardziska-Josifovska M (2000) Atomic force microscopy and scanning electron microscopy study of MgO (110) surface faceting. *Surf. Sci.* **457**: 326–336.
- 12 Chern G, Huang J J, and Leung T C (1998) Atomic force microscopy study of the faceting on MgO(110) surface. *J. Vac. Sci. Technol.* **A16**: 946–949.
- 13 Gajdardziska-Josifovska M, Crozier P A, and Cowley J M (1991) A ( $\sqrt{3} \times \sqrt{3}$ ) R30° reconstruction on annealed (111) surfaces of MgO. *Surf. Sci. Lett.* **248**: L259–L264.
- 14 Crozier P A, Gajdardziska-Josifovska M, and Cowley J M (1992) Preparation and characterization of MgO surfaces by reflection electron microscopy. *Microsc. Res. Tech.* **20**: 426–438.
- 15 Plass R, Egan K, Collazo-Davila C, Grozea D, Landree E, Marks L D, and Gajdardziska-Josifovska M (1998) Cyclic ozone identified in magnesium oxide (111) surface reconstructions. *Phys. Rev. Lett.* **81**: 4891–4894.
- 16 Ventrice C A Jr, Bertrams T, Hannemann H, Brodde A, and Neddermeyer H (1994) Stable reconstruction of the polar (111) surface of NiO on Au (111). *Phys. Rev. B* **49**: 5773–5776.
- 17 Hannemann H, Ventrice C A Jr, Bertrams T, Brodde A, and Neddermeyer H (1994) Scanning tunneling microscopy on the growth of ordered NiO layers on Au (111). *Phys. Stat. Sol. (a)* **146**: 289–297.
- 18 Cappus D, Hassel M, Neuhaus E, Heber M, Rohr F, and Freund H-J (1995) Polar surfaces of oxides: reactivity and reconstruction. *Surf. Sci.* **337**: 268–277.
- 19 Barbier A and Renaud G (1997) Structural investigation of the NiO (111) single crystal surface. *Surf. Sci. Lett.* **392**: L15–L20.
- 20 Barbier A, Renaud G, Mocuta C, and Stierle A (1999) Structural investigation of the dynamics of the NiO (111) surface by GIXS. *Surf. Sci.* **433–435**: 761–764.
- 21 Barbier A, Mocuta C, Kuhlbeck H, Peters K F, Richter B, and Renaud G (2000) Atomic structure of the polar NiO (111)- $p(2 \times 2)$  surface. *Phys. Rev. Lett.* **84**: 2897–2900.
- 22 Schofield M (1999) *Electron Microscopy Studies of Zirconia-Alumina Nanolaminates and Nickel Oxide Surfaces*. (Ph.D. Dissertation, University of Wisconsin, Milwaukee.)
- 23 Wolf D (1995) Structure of ionic interfaces from an absolutely convergent solution of the Madelung problem. *Solid State Ionics* **75**: 3–11.
- 24 Oliver P M, Watson G W, and Parker S C (1995) Molecular-dynamics simulations of nickel oxide surfaces. *Phys. Rev. B* **52**: 5323–5329.
- 25 Watson G W, Kelsey E T, deLeeuw N H, Harris D J, and Parker S C (1996) Atomistic simulation of dislocations, surfaces, and interfaces in MgO. *J. Chem. Soc. Faraday Trans. II* **92**: 433–438.
- 26 Cappus D, Xu C, Ehrlich D, Dillmann B, Ventrice C A Jr, Al-Shamery K, Kuhlbeck H, and Freund H J (1993) Hydroxyl groups on oxide surfaces: NiO(100), NiO(111) and Cr<sub>2</sub>O<sub>3</sub>(111). *Chem. Phys.* **177**: 533–546.
- 27 Rohr F, Wirth K, Libuda J, Cappus D, Baumer M, and Freund H J (1994) Hydroxyl driven reconstruction of the polar NiO(111) surface. *Surf. Sci.* **315**: L977–L982.
- 28 Langell M A and Nassir M H (1995) Stabilization of NiO(111) thin films by surface hydroxyls. *J. Phys. Chem.* **99**: 4162–4169.
- 29 Gajdardziska-Josifovska M, Plass R, Pauli M, Saldin D K, and Chambers S A (2000) X-ray photoelectron spectroscopy and diffraction studies of the polar MgO(111)-(1 × 1) surface (in preparation).
- 30 Tsukada M and Hoshino T (1982) On the electronic structure of the polar surface of compound crystals. *J. Phys. Soc. Jpn.* **51**: 2562–2567.
- 31 Gibson A, Haydock R, and LaFemina J P (1992) Electronic structure and relative stability of the MgO (001) and (111) surfaces. *J. Vac. Sci. Technol.* **10**: 2361–2366.
- 32 Goniakowski J and Noguera C (1995) Atomic and electronic structure of steps and kinks on MgO(100) and MgO (110). *Surf. Sci.* **340**: 191–204.
- 33 Pease W R, Segall R L, Smart R St C, and Turner P S (1980) Evidence for modification of nickel oxide by silica. *J. C S Faraday I* **76**: 1510–1519.
- 34 Cowley J M (1982) Surface energies and surface structure of small crystals studied by use of a STEM instrument. *Surf. Sci.* **114**: 587–606.
- 35 Ignatiev A, Lee B W, and Van Hove M A (1977) *Proc. 7<sup>th</sup> IVC and 3<sup>rd</sup> ICSS* (Vienna), p. 2435.
- 36 Van Hove M A and Enchenique P M (1979) On layer spacing relaxations at surfaces of ionic crystals. *Surf. Sci.* **82**: L298–L300.
- 37 Gajdardziska-Josifovska M, Crozier P A, McCartney M R, and Cowley J M (1993) Ca segregation and step modifications on cleaved and annealed MgO (100) surfaces. *Surf. Sci.* **284**: 186–199.
- 38 Crozier P A and Gajdardziska-Josifovska M (1993) Reflection electron energy loss studies of Ca segregation on MgO (100) surfaces. *Ultramicroscopy* **48**: 63–76.
- 39 Takayanagi K, Tanishiro Y, Takahashi M, and Takahashi S (1985) Structure analysis of Si(111)-7 × 7 reconstructed surface by transmission electron diffraction. *Surf. Sci.* **164**: 367–392.
- 40 Marks L D, Bengu E, Collazo-Davila C, Grozea D, Landree E, Leslie C, and Sinkler W (1998) Direct methods for surfaces. *Surf. Rev. Lett.* **5**: 1087–1106.
- 41 Xu P, Jayaram G, and Marks L D (1994) Cross-correlation method for intensity measurements of transmission electron-diffraction patterns. *Ultramicroscopy* **53**: 15–18.
- 42 Schofield M A, Plass R A, Grozea D, Bengu E, Hardcastle S, and Gajdardziska-Josifovska M (2000) Structure determination of the polar NiO(111)-( $\sqrt{3} \times \sqrt{3}$ )R30 surface reconstruction using direct methods for transmission high-energy electron diffraction (in preparation).
- 43 Yeadon M, Yang J C, Averbach R S, and Gibson J M (1998) Sintering and oxidation using a novel ultrahigh vacuum transmission electron microscope with *in situ* magnetron sputtering. *Microsc. Res. Tech.* **42**: 302–308.
- 44 Sharma R, Gai P L, Whitman L J, Gajdardziska-Josifovska M, and Sinclair R (eds) (1996) *In Situ Electron and Tunneling Microscopy of Dynamic Processes, MRS Proceedings*, Vol. 404.
- 45 Sharma R, Weiss K, McKelvy M, and Glaunsinger W (1994) Gas reaction chamber for gas-solid interaction studies by high resolution transmission electron microscopy. In: *Proc. 52nd Ann. Meet. Microscopy Society of America*, pp. 494–495.
- 46 Sharma R and Weiss K (1998) Development of a TEM to study *in situ* structural and chemical changes at atomic level during gas-solid interactions at elevated temperatures. *Microsc. Res. Technol.* **42**: 270–280.
- 47 Gajdardziska-Josifovska M and Sharma R (2000) EREM and ETEM study of oxygen and hydrogen interaction with hot NiO(100) and NiO(111) surfaces (in preparation).